Solar Neutrino Precision Measurements using all 1496 Days of Super-Kamiokande-I Data

M. B. Smy[a] (for the Super-Kamiokande Collaboration)

[a] Department of Physics and Astronomy,
University of California, Irvine,
Irvine, California 92697, USA

The results of the entire Super-Kamiokande-I solar neutrino data are presented. The measured interaction rate is $47 \pm 2\%$ of the rate expected by the standard solar model and $133 \pm 5\%$ of the rate implied by the SNO charged-current interaction rate. There is no evidence for spectral distortion or a time dependent neutrino flux. Together with the rates of other experiments, the Super-Kamiokande results imply active solar neutrino oscillations and restrict neutrino mixing and mass square difference to lie within the LMA solution area.

1. Introduction

Between May 31$^{\rm st}$, 1996 and July 15$^{\rm th}$, 2001 Super-Kamiokande (SK) exposed 22,500 tons of purified water for 1496 days to solar neutrinos. The detector is described elsewhere [1]. Solar neutrinos are detected using the Cherenkov light emitted by the recoiling electron from neutrino-electron elastic scattering. This water Cherenkov detection technique offers four advantages: (i) the reconstructed direction of the recoiling electron is strongly correlated with the neutrino direction, (ii) the time of each neutrino interaction is recorded, (iii) the neutrino spectrum can be inferred from the recoil electron spectrum, and (iv) neutrino-elastic scattering is sensitive to all neutrino flavors, although the cross section for ν_μ and ν_τ is about six to seven times less than for ν_e. However, only high energy solar neutrinos can be observed in this fashion; SK analyzes data above a threshold of 5 MeV of the total energy of the recoil electron. Only extremely few solar neutrinos have an energy that high; they arise from the β^+ decay of ^{8}B (^{8}B neutrinos) and ^{3}He-proton fusion (*hep* neutrinos) in the sun. The standard solar model (SSM) prediction of the flux of those rare neutrinos ($\phi_{^8B} = 5.05^{+1.01}_{-0.81} \times 10^6/\mathrm{cm}^2\mathrm{s}$ and $\phi_{hep} = 9.3 \times 10^3/\mathrm{cm}^2\mathrm{s}$ with no uncertainty given [2]) is therefore difficult and beset by large uncertainties.

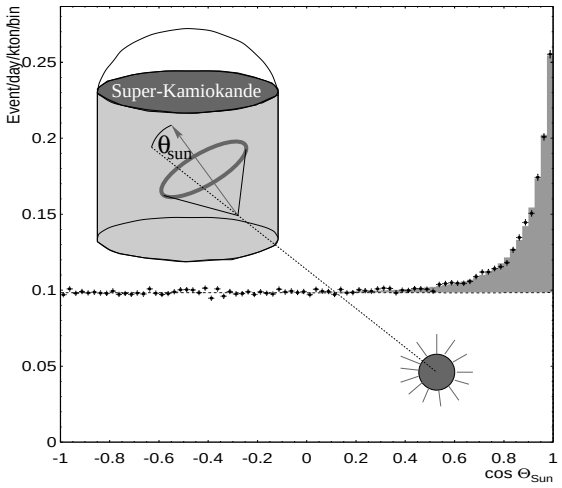

Figure 1. Angular Distribution of Solar Neutrino Event Candidates.

2. Solar Neutrino Flux

SK uses the known position of the sun (at the time of a solar neutrino event candidate) to statistically separate solar neutrino interactions from background events. During 1496 effective days 22,400±800 solar neutrino inter-

actions were found in the gray shaded forward peak of Figure 1. From Monte Carlo calculations based on the SSM, $48{,}200^{+9,600}_{-7,700}$ are expected. In spite of the large neutrino flux uncertainty, the elastic scattering rate is significantly less than expected from the SSM. The suppression factor Data/SSM MC is about 3σ less than one: $0.465\pm0.005(\text{stat.})^{+0.016}_{-0.015}(\text{syst.})^{+0.19}_{-0.17}(\text{SSM})$. All solar neutrinos are born as ν_e in the sun; if all solar neutrinos *detected by SK* are ν_e's as well then a ν_e flux of $2.35\pm0.02(\text{stat.})\pm0.08(\text{syst.})\times10^6/\text{cm}^2\text{s}$ leads to the observed interaction rate.

SNO has measured the charged-current interaction rate of solar ν_e with deuterium [3] (above a threshold neutrino energy of about 7 MeV) implying a ν_e flux of $1.76^{+0.06}_{-0.05}(\text{stat.})\pm0.10(\text{syst.})$ (assuming an undistorted ^{8}B neutrino spectrum) and consequently $16{,}800^{+1,100}_{-1,000}$ ν_e interactions in SK. SK has observed $1.334\pm0.013(\text{stat.})^{+0.047}_{-0.043}(\text{syst.})^{+0.066}_{-0.061}(\text{SNO})$ more events which is about 4.5σ above one.

Beyond the ^{8}B endpoint of ≈ 15 MeV, *hep* neutrinos dominate the solar neutrino flux. Taking into account energy resolution, an optimum *hep* neutrino search window (18 to 21 MeV) was defined using Monte Carlo. In that window 4.9 ± 2.7 events were observed; one *hep* neutrino interaction is expected. This limits the *hep* flux to be less than $73\times10^3/\text{cm}^2\text{s}$ (or less than 7.9 times the SSM flux) at 90% C.L.

3. Solar Antineutrinos

If there are antineutrinos in the solar ν flux, they could be detected by an inverse β reaction on hydrogen. Unlike elastic scattering (as shown in Figure 1, those events are reconstructed within about 60^0 of the forward direction), the angular distribution of this reaction is essentially flat, with a slight backward bias, especially for low energy neutrinos. The positron energy is strongly correlated with the antineutrino energy. After solar neutrino interactions are removed using an angular cut of 60^0, the dominant background at higher energy (above 8 MeV) is due to cosmic ray-induced spallation. Figure 2 shows two upper flux limits at 90% C.L.: (i) all events below $\cos\theta_{\text{sun}} < 0.5$ are considered to be antineutrino

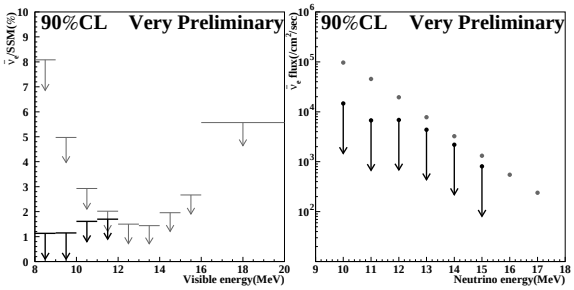

Figure 2. Energy-Dependent Upper Limit of $\overline{\nu_e}$ at 90% C.L. The left panel assumes the ^{8}B spectrum, the right panel uses monochromatic neutrinos at eight energies. The black data points statistically subtract spallation background.

interactions (ii) spallation background is statistically subtracted. The limits of the left plot (in % of the SSM ^{8}B flux) assume antineutrinos with a ^{8}B energy spectrum, the limits given in the right plot (in $/\text{cm}^2\text{s}$) are for monochromatic antineutrinos of eight different energies.

4. Time Variations

Figure 3 shows the time variation of the neutrino flux inferred from the SK rate in bins of ten days and 1.5 months. A 7% yearly variation is expected due to the 3.5% change in distance between sun and earth (assuming the neutrino flux is proportional to the inverse square of this distance, that is, the sun is a neutrino point source). The data favor such a 7% variation over no variation by about 2.5σ. No significant time variation is seen after subtraction of this effect. To search for daily variation, the data was binned according to solar zenith angle θ_z. Figure 4 displays the resulting distribution. No significant daily variation is found. The result can be summarized by forming the "day/night asymmetry" $A_{DN} = \frac{D-N}{0.5(D+N)}$ (with D meaning "day rate" and N meaning "night rate"): $A_{DN} = -0.021 \pm 0.020(\text{stat.})^{+0.013}_{-0.012}(\text{syst.})$ is consistent with zero within 0.9σ.

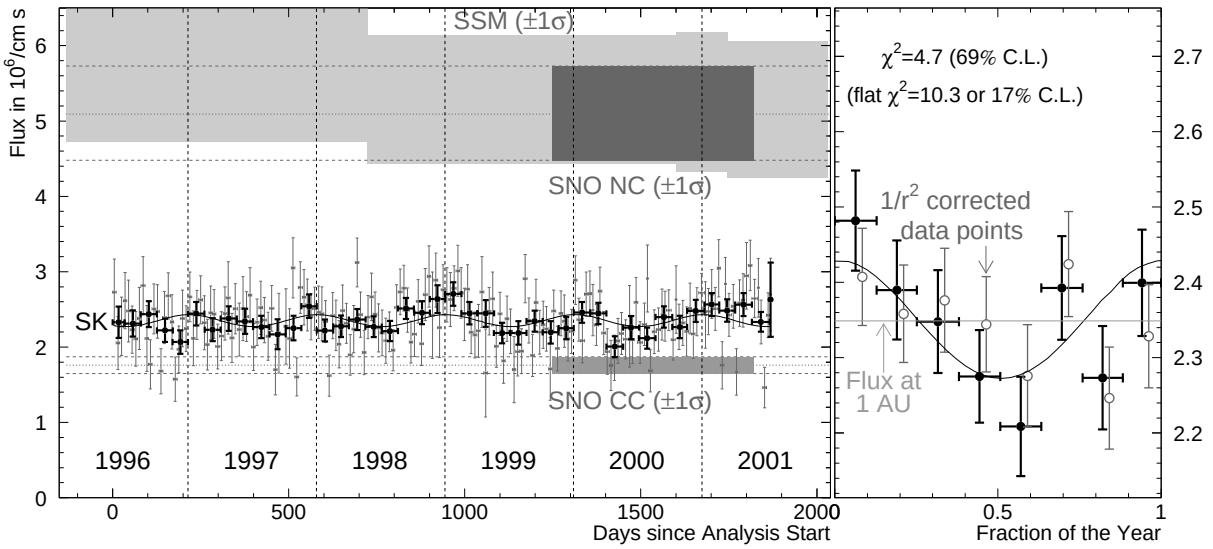

Figure 3. Time Variation of the SK Elastic Scattering Flux. The gray data points are measured every 10 days, the black data points every 1.5 months. The SSM prediction is indicated by the gray band; also shown are the SNO charged-current and neutral-current measurements. The black line indicates the expected annual 7% flux variation. The right-hand panel combines the 1.5 month bins to search for yearly variations; the vertical scale is ten times larger and the zero suppressed. The gray data points (open circles) are obtained from the black data points by subtracting the expected 7% variation.

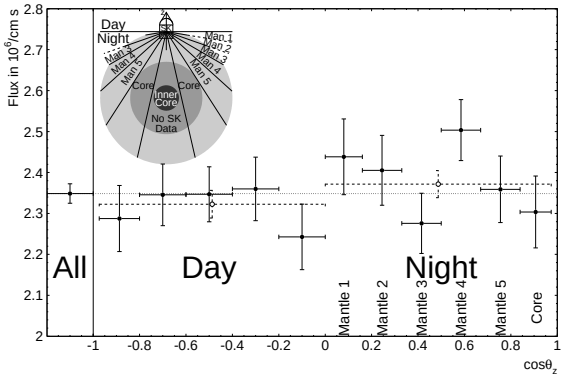

Figure 4. Elastic Scattering Flux as a Function of Solar Zenith Angle. Note the suppressed zero.

5. Spectrum

For precision measurements of the spectrum it is necessary to calibrate the absolute energy scale (and determine the energy resolution) of SK with an outside source. We employed an electron linear accelerator to determine the energy scale within 0.64% and the resolution within 2.5% [1]. In Figure 5 the observed recoil electron spectrum is compared to the expected spectrum: the ratio *Data/SSM* effectively plots spectral distortion. There is no significant spectral distortion; the fit to the no-distortion hypothesis results in $\chi^2 = 20.2/20$ d.o.f. corresponding to 44.3% C.L. The χ^2 includes three systematic effects which will shift all bins of the distribution in a correlated way (correlated uncertainties): the uncertainty in (i) the ^{8}B ν spectrum, (ii) the ab-

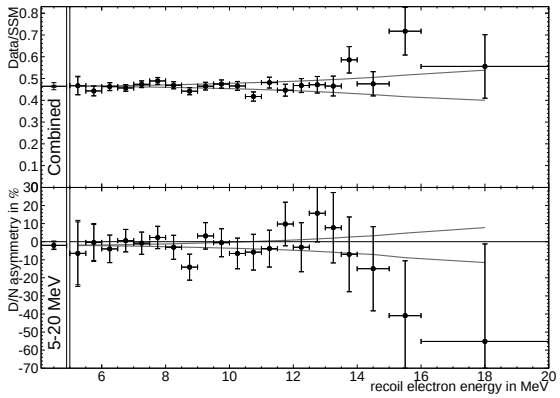

Figure 5. Rate Suppression (Upper Panel) and Day/Night Asymmetry (Lower Panel) as a Function of Energy. The smaller error bars of each data point show the statistical, the larger error bars the combined uncorrelated uncertainty. The gray lines are the $\pm 1\sigma$ correlated uncertainty due to the uncertainty in the ^{8}B ν spectrum and the SK energy scale and resolution. All data points are dominated by statistical uncertainty except the combined rate.

solute SK energy calibration, and (iii) the SK energy resolution. The gray lines of Figure 5 show the size of the sum (in quadrature) of (i), (ii) and (iii). The same figure also plots the day/night asymmetry as a function of recoil electron energy. The day/night asymmetry is consistent with zero regardless of the recoil electron energy. The plotted correlated uncertainty is the sum of only (ii) and (iii), since (i) is the same for the day and the night.

6. Effects of Solar Neutrino Oscillations

Solar neutrino oscillations explain both the observed SK rate reduction compared to the SSM prediction *and* the observed SK rate enhancement relative to the SNO-based expectation (mentioned in section 2) as conversion of ν_e into other active flavors, that is ν_μ or ν_τ. They also explain the rates observed by various radio-chemical solar neutrino experiments [4–6]. Solar neutrinos are always born as ν_e; their conversion probability into ν_μ or ν_τ in vacuum is determined by their energy and the distance of flight and the oscillation parameters. For the purpose of this paper, we assume just two massive neutrinos; in that case the oscillation parameters are the mixing angle θ (controlling the relationship between flavor and mass eigenstates) and the differences of the squared masses between the two neutrinos Δm^2.

The presence of matter strongly influences this conversion probability. In particular, the matter density in the sun is high enough to induce resonant conversion [7] at solar neutrino energies for a wide range of Δm^2 (10^{-8} to 10^{-4}eV^2). In that case, the conversion probability is large or even maximal, even if the mixing angle is small. The matter density in the earth also affects the conversion probability leading to apparent daily variations of the solar neutrino flux.

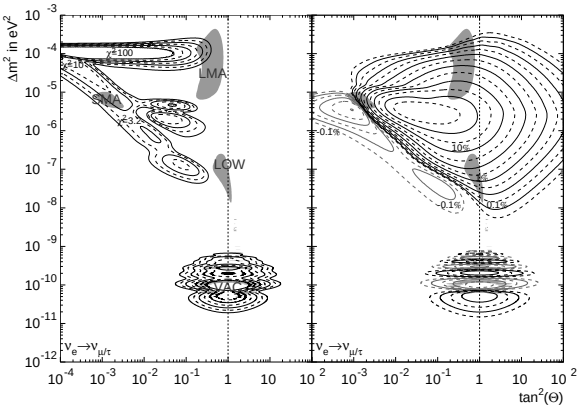

Figure 6. Oscillation Predictions of SK Spectral Distortion (Left) and Day/Night Asymmetry (Right). The spectral distortion is depicted in contours of equal χ^2. The shown values of both the χ^2 and the day/night asymmetry contours increase logarithmically. Superimposed in gray are the usual solution areas.

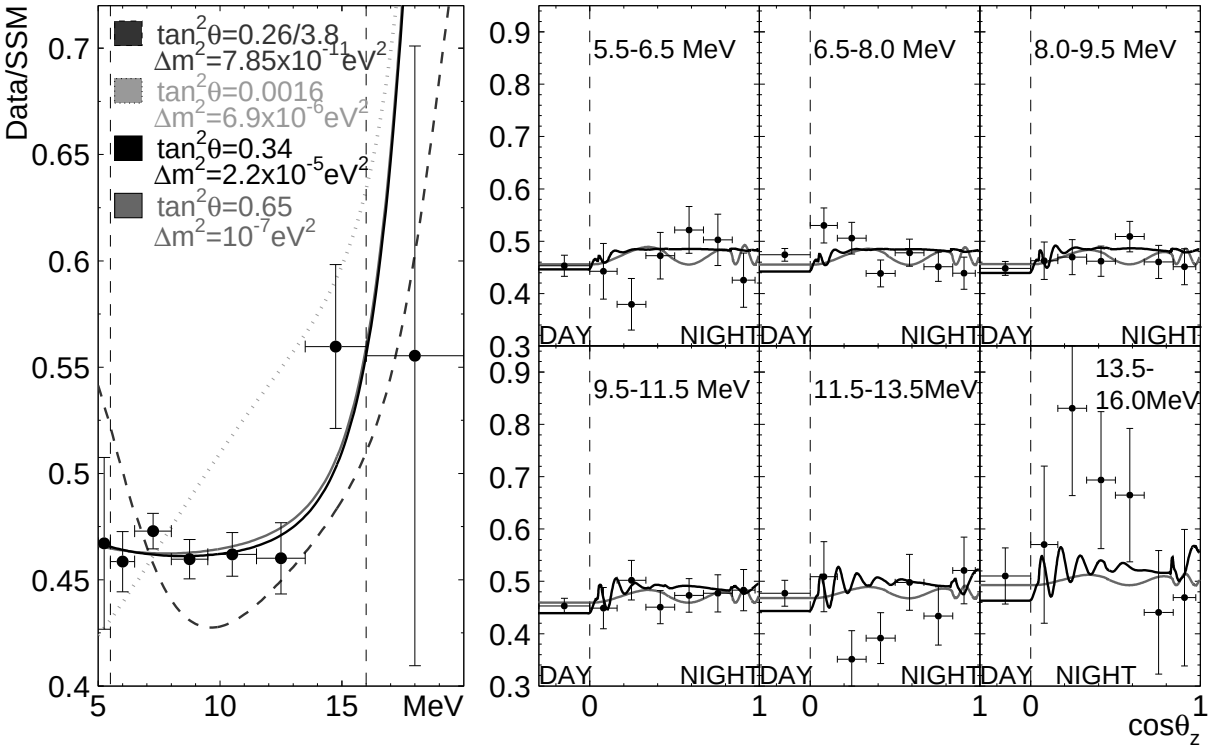

Figure 7. Zenith Spectrum and Four Oscillation Predictions. SMA (dotted line) and VAC (dashed line) solutions are disfavored by spectral distortion data, LOW (light gray) solutions by the absence of solar zenith angle variation. The LMA solutions (black) fit best.

Depending on θ and Δm^2, SK can therefore observe distortions of the recoil electron spectrum, yearly variations or daily variations. In Figure 6, the expected spectral distortion and day/night asymmetry are shown for all values of $\tan^2\theta$ and Δm^2 (The spectral distortion is quantified by a χ^2 method which uses the current SK uncertainties as input). Overlaid are the traditional oscillation "solutions", an area of parameter space capable of explaining all measured solar neutrino rates. The conversion probabilities for the large mixing angle (LMA), small mixing angle (SMA) and low Δm^2 (LOW) solutions are dominated by the matter effects mentioned previously, while the vacuum solutions (VAC) match the first oscillation phase maximum to the solar neutrino energy range. LMA, LOW and VAC have a large mixing angle close to $\pi/4$ while the mixing of the SMA is small (a few 10^{-2}). SMA and VAC solutions predict a distorted spectrum, LMA and LOW solutions daily variations.

Figure 7 summarizes the data used for a simultaneous search for spectral distortions and daily variations: the zenith angle spectrum has eight energy bins and seven solar zenith angle bins between 5.5 and 16 MeV. The χ^2 for a flat shape hypothesis is $\chi^2 = 40.5/43$ d.o.f. which corresponds to 58.1% C.L. Overlaid are the oscillation predictions (fit to the data by varying freely the total ^{8}B and *hep* neutrino flux) for four selected parameter pairs, each representing a solution. The strong energy dependence of the flavor conversion (inducing spectral distortions) predicted by VAC and SMA is not supported by the data. In case

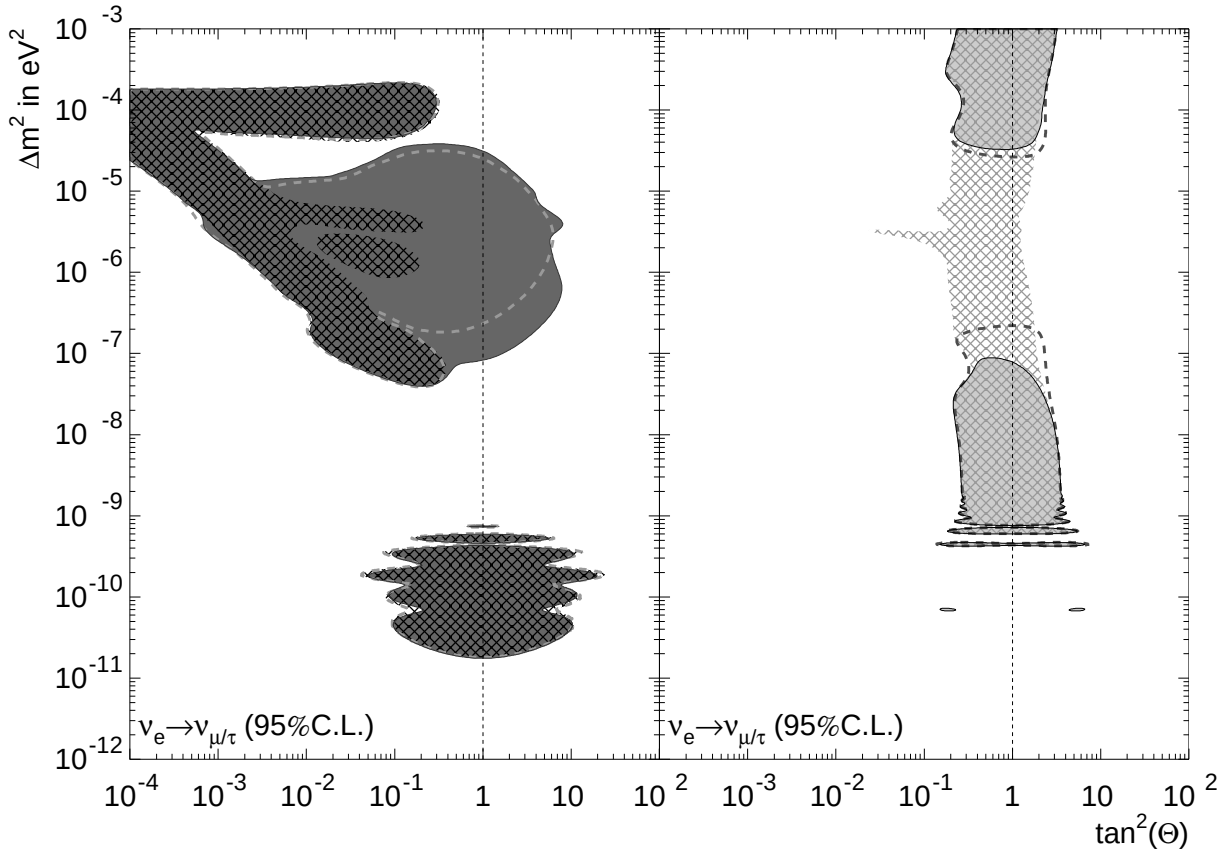

Figure 8. SK Excluded (Left) and Allowed (Right) Regions at 95% C.L. The cross hatched areas use the SK spectrum, the inside of the dashed lines the shape of the SK day/night spectrum (see Figure 5). The shaded areas use the zenith angle spectrum. To get the allowed regions on the right, the shape is combined with the SK rate and the SSM constraint on the ^{8}B flux.

of LMA and LOW, there is little energy dependence of the flavor conversion, the apparent spectral distortion shown in Figure 7 is caused by a larger ratio of the *hep* to the ^{8}B neutrino flux than predicted in the SSM. These two solutions can only be distinguished by their daily flux variation predictions. LMA shows rapid oscillations during the night. These oscillations are washed out for the coarse bins of the data. The LOW solutions however predict *slow* oscillations in the night. The statistical fluctuations of the observed flat distributions would be more consistent with slow oscillations of the opposite phase.

7. Oscillation Analysis

Figure 8 shows the strong constraints on solar neutrino oscillation parameters which are imposed by the SK spectral distortion data (cross hatched areas) and the SK zenith angle spectrum (gray areas). A fit to two spectra (day and night; see gray dashed lines) *partially* includes the zenith angle variation which is *fully* included in the zenith angle spectrum fit. The analysis is described in [8]; the definition of the χ^2 employed to extract those constraints can be found in [9]. The areas in the left panel of Figure 8 are excluded and use only the (zenith angle) spectrum

shape while the right panel shows allowed areas based on this shape *and* the SK rate (and the SSM ^{8}B flux). SK rate and spectrum allow only large mixing angles. The large daily variation predicted between $\approx 10^{-5}$ and $\approx 10^{-7}$eV^2 splits this "large mixing band" into two distinct allowed areas (SK LMA and SK LOW/quasi-VAC). The Δm^2 limits of these areas are stronger for the zenith angle spectrum compared to the day/night spectrum, especially the upper limit for the SK LOW/quasi-VAC which is reduced by a factor of two to three.

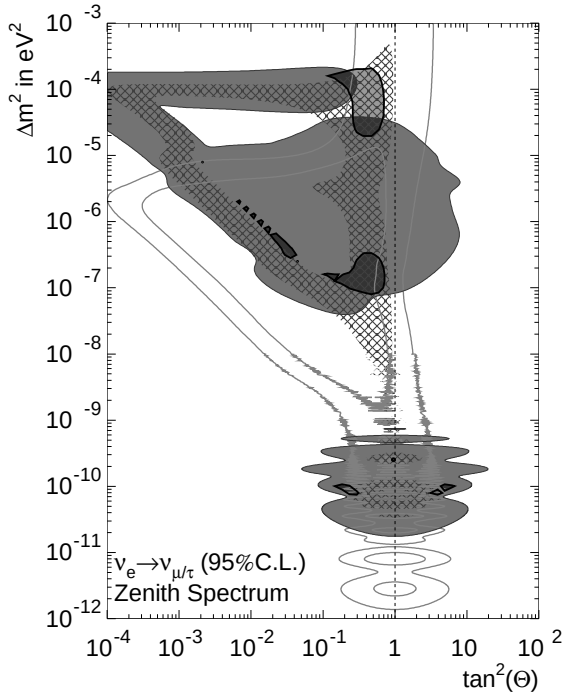

Figure 9. Area Excluded at 95% C.L. by the Shape of the SK Zenith Spectrum (Gray Area). The exclusion is independent of all SSM ν flux predictions. Overlaid is the allowed area (inside thick black line shaded in light gray) from the SNO day/night spectrum [10]. The overlap of both is shaded dark gray. The cross hatched area is allowed by the rate of the Homestake experiment [4] and the SSM prediction of that rate. Similarly, the gray lines mark the boundary of the area allowed by Gallex/GNO [5] and SAGE [6].

Figure 9 compares the constraints of the zenith angle spectrum (gray area) with the allowed areas of the SNO day/night spectrum [10], the Homestake experiment and the combined "Gallium experiments" (Gallex/GNO and SAGE). All SNO small angle ($\tan^2\theta < 0.1$; in particular the one at $\tan^2\theta = 0.002$, which is consistent with the Gallium experiments), VAC (consistent with Homestake and the Gallium experiments, including the one at $\tan^2\theta = 1$), and LOW solutions (consistent with Homestake and the Gallium experiments) are excluded. The SNO LMA solutions (consistent with all experiments) are restricted to a smaller range. The zenith angle spectrum also excludes almost the entire Homestake allowed area (except for LMA and the region just below the LOW solutions).

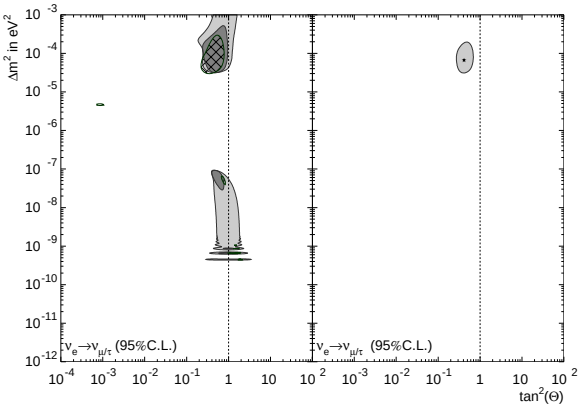

Figure 10. Combined Allowed Regions. The light gray area on the left is allowed by the shape of the SK zenith angle spectrum combined with the SK rate and the SNO charged-current rate. The fit leading to the dark gray area includes in addition the SNO neutral-current rate. The cross hatched allowed area results from a combined fit of the SK zenith angle spectrum and the Gallium, Homestake and SK rates together (and the SSM ν flux predictions). The right panel shows the results of a fit to all solar neutrino data using the SSM ν flux predictions except for the ^{8}B and *hep* fluxes.

8. Combined Oscillation Fits

Stronger constraints on neutrino oscillation parameters can be obtained when the SK results are combined with other solar neutrino data. In particular, for the first time, a *unique* solution is obtained, when SK results are combined with all other solar neutrino data [9]. The strongest constraints that are independent of SSM neutrino flux predictions come from fits which combine the SK zenith spectrum shape with the SK and SNO rates [11]. The left plot of Figure 10 shows the allowed regions of this fit. Superimposed is a combined fit of the SK zenith spectrum shape and the Gallium, Homestake and SK rates which relies on the SSM neutrino flux predictions. In either case only large mixing angle solutions survive. The LMA solutions are favored in either case. When all solar neutrino data is combined, the LMA solutions are more strongly favored.

Figure 11 plots the χ^2 difference $\Delta\chi^2$ as a function of only one parameter for various fits. (The other parameter is chosen as to minimize χ^2.) $\Delta\chi^2$ has the statistics of a χ^2 with one degree of freedom. SK data by itself strongly disfavors small mixing. LMA solutions are favored, however quasi-VAC solutions (between LOW and VAC) provide reasonable fits as well with small "pockets" of parameter space that fit even better than LMA solutions. The SK-SNO combined fit favors the LMA at the 2σ level and tightens the allowed range in the mixing angle. The SK-Gallium-Homestake combined fit disfavors LOW and quasi-VAC solutions more strongly, but SMA solutions are only disfavored by 2 to 2.5σ. The all-combined fit favors the LMA by almost 3σ with small allowed ranges in $\tan^2\theta$ and Δm^2.

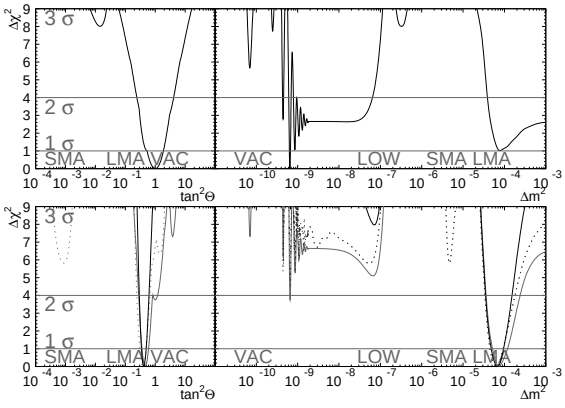

Figure 11. Difference in χ^2 as a Function of $\tan^2\theta$ (left) and Δm^2 (right). The top plots show only the fit to the SK data and the SSM. The bottom plots contain the fit to all solar data (black solid line), the fit to SK and SNO data (gray solid line) and the fit to Homestake, Gallex/GNO, SAGE and SK data (and the SSM; gray dotted line).

9. Conclusion

Super-Kamiokande solar neutrino precision measurements provide the first hint of solar neutrino flavor conversion due to oscillation in a *unique* parameter region, the LMA solution. Solar neutrino oscillation parameters that lead to significant distortions of the ^{8}B neutrino spectrum or solar zenith angle variations are excluded by Super-Kamiokande data.

REFERENCES

1. M. Nakahata et al., Nucl. Instrum. Methods A 421, 113 (1999).
2. J.N. Bahcall, M.H. Pinsonneault, S. Basu, Astrophys. J. 555, 990 (2001).
3. Q.R. Ahmad et al., Phys. Rev. Lett. 89, 011301 (2002).
4. B.T. Cleveland et al., Astrophys. J. 496, 505 (1998).
5. T. Kirsten, reported at this conference
6. V.N. Gavrin, reported at this conference
7. S.P. Mikheyev and A.Y. Smirnov, Sov. Jour. Nucl. Phys. 42, 913 (1985); L. Wolfenstein, Phys. Rev. D 17, 2369 (1978).
8. S. Fukuda et al., Phys. Rev. Lett. 86, 5656 (2001).
9. M.B. Smy, hep-ex/0202020 (2002).
10. Q.R. Ahmad et al., Phys. Rev. Lett. 89, 011302 (2002).
11. M.B. Smy in Neutrino Oscillations in Venice, ed. M. Baldo Ceolin, (Venezia, 2001) 35.